Compressed Sensing for Accelerated EAP Recovery in Diffusion MRI

Sylvain Merlet, Rachid Deriche

Compressed Sensing for Accelerated EAP Recovery in Diffusion MRI

Sylvain Merlet and Rachid Deriche

Athena Project-Team, INRIA Sophia Antipolis - Méditerranée, France

Abstract. Compressed Sensing (CS) or Compressive Sampling is a recent technique to accurately reconstruct sparse signals from under sampled measurements acquired below the Shannon-Nyquist rate. In this article, we present a CS based method for accelerating the reconstruction of the Ensemble Average Propagator (EAP), also known as the Propagator in Diffusion MRI (dMRI), by significantly reducing the number of measurements. Contrarily to the time consuming acquisition technique known as the Diffusion Spectrum Imaging (DSI), our method is developed and implemented to efficiently reconstruct the EAP from reduced and non uniformly under sampled Diffusion Weighted (DW) MRI images combined to an efficient and accurate l_1 norm based reconstruction algorithm. We illustrate in detail the artifacts occurring in a classical EAP reconstruction à la DSI, and qualitatively and quantitatively demonstrate good and better results in recovering the EAP and some of its important features such as the Orientation Distribution Function (ODF) from non-regularly undersampled and l_1 norm based reconstructed data. This opens an original and very interesting road to shorten the dMRI acquisition time and opens new opportunities to render High Angular Resolution Diffusion Imaging (HARDI) feasible in a clinical setting.

Key words: Diffusion MRI; Compressed sensing; Ensemble Average Propagator recovery; Propagator; Orientation Distribution Function

1 Introduction

Diffusion MRI (dMRI) is a recent Magnetic Resonance Imaging technique introduced by [13, 15, 19]. Since the first acquisitions of diffusion-weighted images (DWI) in vivo by [16, 17] and the development of the rigorous formalism of the diffusion tensor (DT) model by [3, 2], dMRI has become an established research tool for the investigation of tissue structure and orientation.

Using dMRI to infer the 3D Ensemble Average Propagator (EAP) also known as the diffusion probability displacement function or propagator (PDF) requires the acquisition of many diffusion images sensitized to different orientations in the sampling space. The number of diffusion weighted images (DWI) required depends on how the diffusion is modeled. The well known DT model assumes the PDF is Gaussian and requires at least 6 DWIs plus an additional unweighted image. However, the Gaussian assumption is an over-simplification of the diffusion of water molecules in the brain and thus has some limitations for voxels in which there is more complicated internal structure.

Therefore, it is of utmost importance to develop techniques that go beyond the limitations of diffusion tensor imaging (DTI). To do so, high angular resolution diffusion imaging (HARDI) has been proposed to measure the diffusion of water molecules along several directions. HARDI depends on the number of measurements N and the gradient strength (b-value), which will directly affect acquisition time and signal to noise ratio in the signal. One way to proceed for the acquisition in HARDI is to sample the whole q-space 3D Cartesian grid. In Diffusion Spectrum Imaging (DSI), a large number of q-space points are taken over the discrete grid and the inverse Fourier transform of the measured DWI signal is taken to obtain an estimate of the diffusion PDF P. The method requires very strong imaging gradients ($500 \leq b \leq 20000$ s/mm^2) and a long time for acquisition (up to 60 minutes) depending on the number of sampling directions, which can be problematic for clinical studies involving children and people afflicted with certain diseases. A large number of acquisitions can force the patient to abort or render the diffusion weighted images useless. According to the literature [11], if established practice is followed, 515 diffusion-weighted images are acquired successively to obtain data of good quality. Each image corresponds to a different q vector, the effective diffusion gradient.

The visualization of 3D diffusion PDF at every voxel is computationally intensive. Hence, people either take an isosurface of the diffusion PDF for a certain radius $\mathbf{r}$ or the diffusion Orientation Distribution Function (ODF) is computed. The diffusion ODF contains the full angular information of the diffusion PDF and is defined as [1, 20]

$$\Psi(\theta, \phi) = \int_0^\infty P(r, \theta, \phi) r^2 dr, \tag{1}$$

where (θ, ϕ) obey physics convention ($\theta \in [0, \pi], \phi \in [0, 2\pi]$).

This is a spherical function which is very useful to drive tractography since it overcomes the limitations of DTI in fiber crossing regions, especially for higher b-value acquisitions with $b \geq 1000$ s/mm^2 [11, 6]. One of the HARDI techniques known as the Q-ball imaging (QBI) [21, 5] consist in sampling the q-space on a single sphere in several directions instead of attempting to get the entire q-space. QBI aims to estimate the ODF directly from the measured signal by means of the Funk-Radon transform (FRT) [21, 1].

However, the ODF only captures angular information of the diffusion process. As explained above, the Diffusion Spectrum Imaging (DSI) technique approximates the ensemble average propagator P by taking samples on the whole q-space. It aims to estimate directly the PDF in a numerical way without any prior knowledge about the tissue shape. This results in estimating the diffusion PDF P in a more accurate fashion than any other methods. Both radial information from DTI and angular information from QBI are caught, that makes DSI a richer technique than QBI [21] or DTI. This method, first attempted by [23], considers that the measured signal, after normalization, is written as the 3-dimensional Fourier transform of the diffusion propagator P [18],

$$E(q) = F[P(r|r_0, \tau)] \tag{2}$$

where q and r are both 3D-vectors that represent respectively the effective gradient direction and the diffusion direction. $E(q) = S(q)/S_0$ is the normalized attenuated diffusion signal expressed as the ratio of the attenuated diffusion signal and the signal measured without any diffusion encoding gradient ($q = 0$). P is the probability that a molecule moves from a position r_0 to r after a delay τ. Using equation 2, it is straightforward to get P by taking the inverse 3D Fourier transform of the signal E measured in the q-space. Many measurements are necessary to obtain high-resolution PDF. In brief, while this technique has the advantage of a very good approximation of the diffusion propagator, it is limited by the long time for acquisition due to the large number of samples required.

Compressed Sensing (CS), a recent technique to accurately reconstruct sparse signals from under sampled measurements acquired below the Shannon-Nyquist rate, HARDI, DSI, the Ensemble Average Propagator and the diffusion ODF play a central role in this work which is focused on the development of CS based method for accelerating the reconstruction of the EAP by significantly reducing the number of acquisitions and measurements.

The method we propose combines the idea of randomly undersampling DW-MRI to the idea of using an efficient and accurate L_1 norm based EAP reconstruction algorithm. Significantly undersampling the q-space in a random fashion and then reconstructing the EAP by solving a convex optimization problem which exploits the sparsity in P is shown to lead to less measurements than needed in DSI and to qualitatively and quantitatively better results in recovering the EAP and some of its important features such as the ODF.

This allows to shorten the dMRI acquisition time, in particular when dealing with High Angular Resolution Diffusion MRI and opens new opportunities to render HARDI feasible in a clinical setting. The next section introduces the CS technique before presenting our L_1 norm based EAP reconstruction algorithm and the experimental results obtained.

2 Signal & Image Reconstruction via Compressed Sensing

The Compressed Sensing (CS) technique has been proving useful in recovering Magnetic resonance images by significantly undersampling their k-spaces [14] [10] [9] [4]. David Donoho described a complete mathematical framework [7] of CS theory. By analogy with the 2D-images case, we know that diffusion propagator P and the attenuated diffusion signal E are related by a 3D Fourier transform (see eq. 2). We use this relation combined with a regularized CS reconstruction to recover P from a small number of measured coefficients.

A fundamental result in signal theory is the Nyquist-Shannon sampling theorem. It indicates the minimum sampling frequency required to avoid aliasing, equal to twice the highest frequency contained within the signal. Undersampling a signal in the Fourier space regardless of this theorem does not enable

to reconstruct the signal that would has been given from all the Fourier coefficients. It produces regular shifted replicas typically resulting in an image of little diagnostic value that does not permit any reconstruction. However, the proposition is valid regarding a regular undersampling scheme. A random undersampling scheme results in incoherent artefacts spread all over the image as a random noise and an appropriate reconstruction method can allow the signal recovering. An example of this phenomenon on a 1-Dimensional signal is shown figure 1(a). We have generated eight signals. The original signal in the top-left is a discrete signal of length 500 and originally sampled at the frequency $f_s = 44100Hz$. We can visualize its Fourier transform on the top-right and see that the maximum frequency component is $f_m = 5000Hz$. Hence, according to the Nyquist-Shannon theorem, the sampling frequency has to respect $f_e > 2f_m$. By returning to the discrete domain, we obtain the Nyquist rate expressed as $N_e = \frac{f_e}{fs} = \frac{2f_m}{f_s} = \frac{2*5000}{44100} = \frac{1}{4.41}$ It indicates the minimum sampling required rate to avoid aliasing. In figure 1 (a), the second and third lines show the signal regularly undersampled but with two different rates and the corresponding Fourier transforms. One respect the Nyquist condition and is undersampled at $N_{u1} = \frac{1}{2} > N_e$ (the second line) and the other violates this condition with a rate $N_{u2} = \frac{1}{6} < N_e$ (the third line). The non-respect of the Nyquist theorem in the second case causes aliasing in Fourier space. This non-reversible phenomenon appears when high frequency components shift and overlay the original frequency components. However, the fourth line of figure 1(a) show a signal undersampled at rate N_{u2}, that is to say without respecting the Nyquist condition, excepted it follows a random undersampling scheme. In this case, we do not see the previous shifted frequency components any more but random-like noise spread all over the signal Fourier transform.

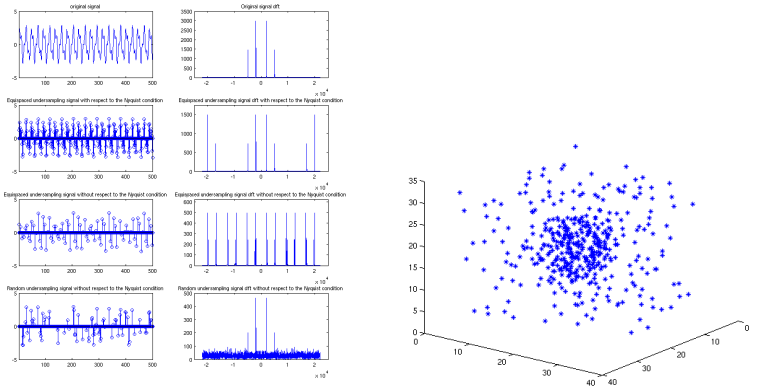

(a) (b)

Fig. 1. (a) Illustration of the Nyquist theorem on a 1D signal and (b) Sampling scheme with 3D binomial distribution.

The possibility to acquire q-space samples in a random fashion is an important aspect in DSI that facilitates the application of the CS technique. We will exploit this property to recover the 3 dimensional propagator P.

Our reconstruction is based on the assumption that P has a sparse representation, that is composed by a small number of non-zero coefficients. If we know that most of the signal coefficients are zeros, why do not we exploit this information for reconstructing the signal? Considering the signal sparse, we can constrain most of its components to be zero by minimizing the number of non-zero elements, that is the l_0 norm defined by $\| x \|_0 = \sum_{i=1}^{N} x_i^0$. Nevertheless, minimizing the l_0 norm is difficult and requires combinatorial optimization so we prefer to minimize the l_1 norm defined by $\| x \|_1 = \sum_{i=1}^{N} |x_i|$. l_1 norm is just the sum of the absolute values of every element and [14] proved that when the l_0-minimization have a sparse solution, the l_1-minimization will find it. We need the solution to be sparse either in its original space or in another domain by applying a sparse transform. A sparse domain enables to represent a signal with a smaller number of non-zero elements than originally and thus enforce the sparsity constraint. Many transforms are known to make a signal sparse, for instance we can cite the Wavelet transform, the discrete cosine transform or simply a finite difference transform. It comes to promote sparsity by minimizing $\|\Psi x\|_1$ where Ψ is a sparse transform.

The solution x of our problem is given by solving the following convex optimization problem:

$$argmin_x J(x) = \|TF_{u0}(x) - E_u\|_2^2 + \lambda\|\Psi x\|_1 \tag{3}$$

The first term is the data consistency constraint, $\|\Psi x\|_1$ is the sparsity constraint. λ is the Lagrange parameter that defines the confidence we put in the measured signal E_u. The data consistency constraint enables the solution to remain close to the raw data acquisition. TF_{u0} is the 3D undersampled Fourier operator defined by three operations. The first operation consists in applying a 3D Fourier transform. The latter is undersampled in a random manner. Then, the other coefficients are replaced by zero values. Hence, the acquired data are defined by $E_u = TF_{u0}(P)$ with P the propagator to be recovered. x is the estimated propagator so $TF_{u0}(x)$ is the undersampled Fourier transform of the estimated propagator. Equation (3) finds the sparsest solution that corresponds to the acquired data.

We have seen the three conditions necessary to reconstruct a signal using Compressed Sensing : (1) Possibility to acquire the measurements in a random fashion. (2) The signal has a sparse representation. (3) Reconstruction via a convex optimization problem. The next section reviews these three CS conditions in the case of a 3D signal : The diffusion propagator or EAP.

3 EAP reconstruction via Compressed Sensing

In this section, we present the CS based recosntruction method.

Undersampling Most of the propagator energy is focused on the origin of its Fourier space. This energy corresponds to the low-frequency components, that describes the main features. Hence, it is judicious to sample more these components, or even fully sample them, and take the higher frequency components in a random fashion. The choice of a well appropriate sampling scheme is a open problem that requires an in-depth study. An appropriate scheme can lead to really good reconstructions whereas a bad scheme can make the reconstruction inapplicable. The CS approach recommends to maximize the degree of incoherence during the undersampling process in order to produce noise-like artefact. A way to measure the incoherence is to compute the Point Spread Function [14]. We are currently working on this important problem and among many sampling scheme already tested, we use a density function compact in the centre and decreasing away from the origin. The Binomial and Gaussian distributions are good candidates for such sampling schemes. An example of 3D Binomial distribution is shown figure 1(b).

EAP natural sparsity The trajectory of water molecules can be described by a random walk, i.e. each molecule follows a random path in a 3D space. However, when looking at a set of molecules, one can see that, in a free medium, the averaged displacement follows a Gaussian distribution. It means most of the molecules remain confined around their initial positions. For example, in free water, at $37°C$, with a diffusion coefficient $D = 3.10^9$, and a diffusion time of $50.10^{-3}s$. 32% of the molecules have moved at least at $17\mu m$ whereas only have passed $34\mu m$ [12].

At the scale of a voxel, one models the diffusion by the EAP, $P(r_0|r, \tau)$. P represents the probability that a molecule moves from an initial position r_0 to r after a delay τ. Because of the Gaussian particular nature, the EAP values decrease while moving away from its centre until falling to zero. Thereby, the propagator is already sparse in free medium. When the diffusion is hindered by biological obstacle, as the myelin in the white matter fibres, the molecules displacement is constrained to the milieu. Beside such hindrance the propagator values decrease to zero. This phenomenon emphasizes the sparsity in the original space of P.

Because of the EAP natural sparsity, we choose to not use any sparse transform for the signal reconstruction.

EAP Reconstruction For some reason explained in the previous paragraph, we consider the case where $\Psi = I$. This leads to the following functional to be minimized :

$$argmin_x J(x) = \|TF_{u0}(x) - E_u\|_2^2 + \lambda\|x\|_1 \tag{4}$$

Many techniques have been recently proposed to solve this functional [8, 24]. We are in the process to test some of the most appropriate. Here, and for simplicity, we just illustrate the case where we find the minimizer of this problem by means of a iterative shrinkage-thresholding algorithm (ISTA), where each

iteration involves a shrinkage step. This method avoids the computation of the l_1-norm gradient, and thus overcome the difficulties that occur when we want to compute the derivative of this norm at zero. The general step of ISTA is

$$x_{k+1} = S_\lambda(x_k - 2\alpha\ TF^*_{u0}(TF_{u0}(x) - E_u)) \tag{5}$$

where α is a suitable stepsize and $S_\lambda : \Re^3 \rightarrow \Re^3$ is the 3D soft-thresholding operator defined by

$$S_\lambda(x) = \begin{cases} 0 & if\ |x|\ \leq\ \lambda \\ x - sign(x)\lambda & otherwise \end{cases} \tag{6}$$

For more detail, we refer the interested reader to [8, 24].

4 Experimental results

In this section, we evaluate the performances of our algorithm on a set of synthetic propagator constructed on a Cartesian grid according to the multi-tensor model.

Propagator comparison. Letting P represent the propagator to be recovered and P' the estimated propagator, we compute the Euclidian distance between P and P' over all the q-space grid, normalized by the norm of P given by

$$error(P, P') = \frac{1}{MNL} \sum_{i=1}^{M} \sum_{j=1}^{N} \sum_{k=1}^{L} \frac{|P(i,j,k) - P'(i,j,k)|}{\|P\|_2^2} \tag{7}$$

where M,N,L are the q-space dimension. In this section, we use this criterion to follow the performances of the method.

Angular information. Because P is a $\Re^3 \rightarrow \Re$ function, we cannot observe it directly. Hence, We chose to visualize its ODF by integration of the probability values in a constant solid angle as expressed in eq. 1. This representation points up the angular information about the diffusion [22] [1].

Synthetic data generation The synthetic data are generated using the multi-tensor model. The diffusion signal S is, thus, described as,

$$S(g_i) = \sum_{k=1}^{K} p_k e^{-b_i g_i^T D_k g_i} \tag{8}$$

where a fibre k is defined by a tensor matrix D_k and a weight p_k. g_i and b_i are the encoding gradient direction and intensity, respectively, allowing to sample the entire q-space. This model enables to simulate multi-crossing fibre. The fibre orientations are defined by the tensor matrix D_k and the number of fibre is indicated by T.

In order to evaluate the performance of our algorithm, we need to generate the propagator P. Recalling that the attenuated diffusion signal $S(g)$ is directly related to the diffusion propagator $P(r)$ by a Fourier transform as expressed in equation 2, we need to compute the inverse Fourier transform of $S(g)$ in order to get $P(r)$. It happens that P(r) is also a multi-Gaussian function expressed as ,

$$P(r) = \sum_{k=1}^{K} \frac{1}{\sqrt{(4\pi b)^3 |D_k|}} p_k e^{\frac{-r^T D_k^{-1} r}{4b}} \tag{9}$$

where r is a 3D vector representing the water molecule displacement.

Simulation The CS method is applied on three phantoms generated as described previously from three tensors $D_1 = diag(10^{-6} \times [150\ 150\ 1500])$, $D_2 = diag(10^{-6} \times [1500\ 150\ 150])$, $D_3 = diag(10^{-6} \times [150\ 1500\ 150])$ and three weights $p_1 = p_2 = p_3 = 1$. One is the diffusion propagator of one fibre mades from D_1 and p_1. The second corresponds to a 90° 2-crossing fibers mades from D_1, D_2 and the corresponding weigths. The third one is the sum of three fibers that crosses each other with a 90° angle and each of the three fiber k is defined by one of the covariance matrix D_k and its p_k. All the synthetic propagators are generated on a $M * N * L = 16 * 16 * 16$ cartesian grid with sampling frequency $f_s = 1.5$. The ODFs corresponding to the radial integration over the entire grid ($K = 16 * 16 * 16 = 4096$ equispaced measurements) are shown in figure 2. The reconstruction is evaluated in the next section after taking N measurements within $K_1 = 5 * 5 * 5 = 125$, $K_2 = 6 * 6 * 6 = 216$, $K_3 = 7 * 7 * 7 = 343$ and $K_4 = 8 * 8 * 8 = 512$ on the intial grid. The corresponding rate are $N_{e1} = K/K_1 = 32.7680$, $N_{e2} = K/K_2 = 18.9630$, $N_{e3} = K/K_3 = 11.9417$ and $N_{e4} = K/K_4 = 8$.

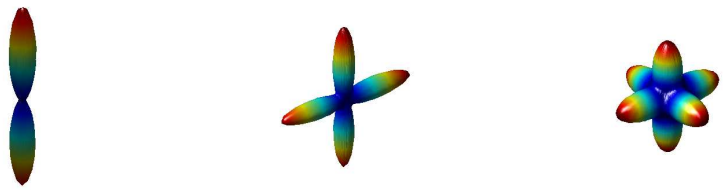

Fig. 2. ODF from 1, 2 and 3 90° crossing fibres propagator

In the first part of the simulation, we take equispaced samples on the grid and try to reconstruct the propagator by computing directly the inverse Fourier transform of the diffusion signal so-undersampled. Table 1 shows numerical results and figure 3 (a) represents the ODFs from the estimated propagator using

DSI. In the second part, the q-space is undersampled in an random fashion using an binomial density function. Then we apply the CS method to recover the propagator. Mean and standard deviation of the error between the true propagator and the estimated propagator are shown table 2 and examples of ODF estimated with our technique are displayed in figure 3 (b).

In a Matlab implementation, the technique proposed take no more than 20 seconds to reconstruct 16*16*16 signal components, on a Intel Core 2 Duo CPU at 2.8 GHz.

The numerical results, shown table 1, indicates that the reconstruction error increases with decreasing number of measurements. We can still reconstruct the propagator in a correct manner with only $N = 512$, in the case of a regular sampling scheme. Below this level the reconstruction error diverges. This is due to the violation of the Nyquist condition. The maximal frequency component for both propagator is $f_m = 6$, so the Nyquist rate is $N_e = 2 * f_m/f_s = 9.333$. The only case where this rate is respected corresponds to the case $N = 512$ measurements.

After randomly undersampling the attenuated diffusion signal and then applying a CS reconstruction, the error between the true propagator and the estimated propagator does not diverge even for a smaller number of measurements (table 2). We note that the regular reconstruction is slightly better for $N = 512$ because the Nyquist theorem is respected. Nevertheless, the DSI reconstruction do not reach the accuracy of a CS reconstruction after this point. Our technique thus overcomes the limitation of DSI concerning the number of measurements.

Standard deviations remain low from $N = 512$ to $N = 216$, which indicates that the reconstruction is quite stable within this range. Below, the lack of precision is due to the random aspect of the method. Indeed, the reconstruction depends on the sampling scheme and we know that an appropriate scheme leads to correct recovering (see sec. 3, Undersampling).

The figure 3 (b) indicates that we can easily extract maxima from all the CS-based estimated ODFs while the DSI-based ODFs presented figure 3 (a) give corrupted angular information from $N = 216$. In spite of unwanted artefacts at $N = 343$ we can still detect maxima. They are regular shifted artefacts that appear when violating the Nyquist conditions. The random undersampling scheme results in incoherent artefacts spread all over the grid as a random noise and the l_1- minimization enables to get rid of it. Once again, the CS reconstruction outperforms the DSI method regarding the recovering of the angular information.

The l1 regularization problem gives large penalty to the small components and tends to produce a solution with a large number of coefficients equal to zero. It results in keeping the coarse features, i.e. the one characterized by the large components. It is exactly what we need to preserve if the signal has a compact, i.e. sparse, representation. The multi tensor model gives a non band-limited signal with many small values away from its centre, which are estimated by zeros after reconstruction. This is not important if we only look at the whole propagator because the small values can be replaced by zero without any prob-

lem. However this phenomenon is emphasized when integrating P values as ODF does. Thereby, the ODF look a bit flattened as an effect of the l1 regularization (fig. 3).

DSI with Regular undersampling				
	N=125	N=216	N=343	N=512
One fibre phantom ($\times 10^{-5}$)	9.742	7.8826	3.1254	1.9459
90° 2-crossing fibres phantom ($\times 10^{-5}$)	17.384	13.113	5.429	1.8143
90° 3-crossing fibres phantom ($\times 10^{-5}$)	16.624	12.944	7.7627	2.6951

Table 1. Error between the true propagator and the estimated propagator for regular undersampling.

DSI with Compressed Sensing based reconstruction and random undersampling				
	N=125	N=216	N=343	N=512
One fibre phantom ($\times 10^{-5}$)	2.8901 ± 0.1413	2.7987 ± 0.0758	2.6214 ± 0.0292	2.5702 ± 0.0178
90° 2-crossing fibres phantom ($\times 10^{-5}$)	3.1131 ± 0.1527	3.007 ± 0.0983	2.9332 ± 0.0364	2.8873 ± 0.0267
90° 3-crossing fibres phantom ($\times 10^{-5}$)	2.9094 ± 0.0495	2.8074 ± 0.0324	2.7239 ± 0.0253	2.7021 ± 0.0203

Table 2. Mean and standard deviation of the error between the true propagator and the estimated propagator.

5 Conclusion

In this article, we have presented a Compressed Sensing based method for accelerating the reconstruction of the Ensemble Average Propagator in Diffusion MRI (dMRI).

It paves the way for a new method to reconstruct the propagator and the subject has to be further developed. We are implementing several optimization techniques in order to solve (4) and some of these techniques seem really promising. The results presented in this article use synthetic data with no noise and, so, do not take in account the perturbations that occur during the acquisition. Hence, our current work considers noisy measurements.

The signal representation has to be compact if we want to reconstruct it. This condition is crucial when we want to decrease the number of measurements

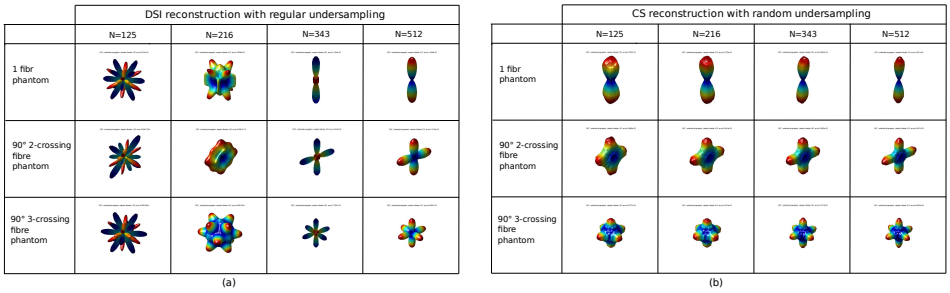

Fig. 3. ODF of the reconstructed propagator on the one fibre phantom and the 90° crossing fibre phantom. (a) CS reconstruction . (b) Direct reconstruction

needed to a good-quality reconstruction. In this paper we have undersampled P to 125 acquisitions because less coefficients are not sufficient to entirely described the propagator. An interesting issue would be to find the transforms which best sparsify P in order to go down the stage of 125 acquisitions.

Aside from these points that need reviews, our method allows to significantly reduce the number of measurements and outperforms the time consuming acquisition technique known as the Diffusion Spectrum Imaging (DSI). Our method efficiently reconstruct the EAP from reduced and non uniformly under sampled Diffusion Weighted (DW) MRI images combined to an efficient and accurate l_1 norm based reconstruction algorithm. This opens an original and very interesting road to shorten the dMRI acquisition time and opens new opportunities to render HARDI feasible in a clinical setting.

Acknowledgement: This work was partially supported by the ANR project NucleiPark.

References

1. i. Aganj, C. Lenglet, and G. Sapiro. Odf reconstruction in q-ball imaging with solid angle consideration,. In *Proceedings of the Sixth IEEE International Symposium Biomedical Imaging, Boston, MA,*, June 2009.
2. P.J. Basser, J. Mattiello, and D. Le Bihan. Estimation of the effective self-diffusion tensor from the nmr spin echo. *Journal of Magnetic Resonance*, B(103):247–254, 1994.
3. P.J. Basser, J. Mattiello, and D. Le Bihan. Mr diffusion tensor spectroscopy and imaging. *Biophysical Journal*, 66(1):259–267, 1994.
4. R. Chartrand. Fast algorithms for nonconvex compressive sensing: Mri reconstruction from very few data. *IEEE International Symposium on Biomedical Imaging (ISBI)*, 2009.
5. M. Descoteaux, E. Angelino, S. Fitzgibbons, and R. Deriche. Regularized, fast, and robust analytical q-ball imaging. *Magnetic Resonance in Medicine*, 58(3):497–510, 2007.

6. Maxime Descoteaux. *High Angular Resolution Diffusion MRI: From Local Estimation to Segmentation and Tractography.* PhD thesis, Nice Sophia Antipolis University,, February 2008.
7. David L. Donoho. Compressed sensing. *IEEE Trans on Information Theory*, 52(4):1, 2004.
8. M. Elad, B. Matalon, J. Shtok, and M. Zibulevsky. A wide-angle view at iterated shrinkage algorithms. In *in SPIE - Wavelet XII*, volume 6701, pages 26–29, August 2007.
9. A. Ganesh, VR Edward, et al. Reordering for improved constrained reconstruction from undersampled k-space data. *International Journal of Biomedical Imaging*, 2008.
10. W. Guoa and W. Yinb. Edgecs: Edge guided compressive sensing reconstruction. 2009.
11. P. Hagmann, L. Jonasson, P. Maeder, J.P Thiran, Van J. Wedeen, and R. Neuli. Understanding diffusion mr imaging techniques: From scalar diffusion-weighted imaging to diffusion tensor imaging and beyond. *RadioGraphics*, 26:S205–S223, 2006.
12. D. Le Bihan. Looking into the functional architecture of the brain with diffusion MRI. *Nature Reviews Neuroscience*, 4(6):469–480, June 2003.
13. D. Le Bihan and E. Breton. Imagerie de diffusion it in vivo par résonnance magnétique nucléaire. *CR Académie des Sciences*, (301):1109–1112, 1985.
14. M. Lustig, D. Donoho, and J.M. Pauly. Sparse mri: The application of compressed sensing for rapid mr imaging. *Magnetic Resonance in Medicine*, 58(6):1182–1195, 2007.
15. K.D. Merboldt, W. Hanicke, and J. Frahm. Self-diffusion nmr imaging using stimulated echoes. *J. Magn. Reson.*, 64:479–486, 1985.
16. M.E. Moseley, Y. Cohen, J. Mintorovitch, J. Kucharczyk, J. Tsuruda, P. Weinstein, and D. Norman. Evidence of anisotropic self-diffusion. *Radiology*, 176:439–445, 1990.
17. P.A. Osment, K.J. Packer, M.J. Taylor, J. J. Attard, T. A. Carpenter, L. D. Hall, S. J. Doran, and N. J. Herrod. Nmr imaging of fluids in porous solids. *Phil. Trans. Roy. Soc.*, 333:441–452, 1990.
18. E.O. Stejskal and J.E. Tanner. Spin diffusion measurements: spin echoes in the presence of a time-dependent field gradient. *Journal of Chemical Physics*, 42:288–292, 1965.
19. D.G. Taylor and M.C. Bushell. The spatial mapping of translational diffusion coefficients by the nmr imaging technique. *Phys. Med. Biol.*, 30:345–349, 1985.
20. A. Tristan-Vega, SC.F. Westin, and S. Aja-Fernandez. Estimation of fiber orientation probability density functions in high angular resolution diffusion imaging. *NeuroImage*, 47(2):638–650, August 2009.
21. D. Tuch. Q-ball imaging. *Magnetic Resonance in Medicine*, 52(6):1358–1372, 2004.
22. V.J. Wedeen, P. Hagmann, W. Tseng, T.G. Reese, and R.M. Weisskoff. Mapping complex tissue architecture with diffusion spectrum magnetic resonance imaging. *Magnetic Resonance in Medicine*, 54(6):1377–1386, 2005.
23. V.J. Wedeen, T. G. Reese, D.S. Tuch, M.R. Weigel, J.-G. Dou, R.M. Weiskoff, and D. Chessler. Mapping fiber orientation spectra in cerebral white matter with fourier-transform diffusion mri. In *Proceedings of the International Society for the Magnetic Resonance in Medecine: 8th Scientific Meeting and Exhibition*, number 82, 2000.
24. M. Zibulevsky and M. Elad. L1-l2 optimization in signal and image processing. *IEEE Signal Processing Magazine*, 27(3), May 2010.